# Rapid #: -9630791

CROSS REF ID: **233181**

LENDER: **IYU :: Main Library**

BORROWER: **TSC :: Cook Library**

| | |
|---|---|
| TYPE: | Article CC:CCG |
| JOURNAL TITLE: | Philosophical magazine |
| USER JOURNAL TITLE: | Philosophical Magazine |
| ARTICLE TITLE: | Novel aspects of charge and lattice dynamics in the hole-doped manganite La0.67Sr0.33MnO3 |
| ARTICLE AUTHOR: | |
| VOLUME: | 95 |
| ISSUE: | 19 |
| MONTH: | |
| YEAR: | 2015 |
| PAGES: | 2078-2091 |
| ISSN: | 1478-6435 |
| OCLC #: | |

Processed by RapidX: 9/9/2015 11:30:02 AM

Taylor & Francis
Taylor & Francis Group

Philosophical Magazine

ISSN: 1478-6435 (Print) 1478-6443 (Online) Journal homepage: http://www.tandfonline.com/loi/tphm20

# Novel aspects of charge and lattice dynamics in the hole-doped manganite $La_{0.67}Sr_{0.33}MnO_3$

**Peng Xu, T.J. Huffman, N.C. Branagan, M.M. Qazilbash, P. Srivastava, T. Goehringer, G. Yong, V. Smolyaninova & R. Kolagani**

**To cite this article:** Peng Xu, T.J. Huffman, N.C. Branagan, M.M. Qazilbash, P. Srivastava, T. Goehringer, G. Yong, V. Smolyaninova & R. Kolagani (2015) Novel aspects of charge and lattice dynamics in the hole-doped manganite $La_{0.67}Sr_{0.33}MnO_3$, Philosophical Magazine, 95:19, 2078-2091, DOI: 10.1080/14786435.2015.1049235

**To link to this article:** http://dx.doi.org/10.1080/14786435.2015.1049235

Published online: 08 Jun 2015.

*Philosophical Magazine*, 2015
Vol. 95, No. 19, 2078–2091, http://dx.doi.org/10.1080/14786435.2015.1049235



# Novel aspects of charge and lattice dynamics in the hole-doped manganite $La_{0.67}Sr_{0.33}MnO_3$

Peng Xu[a], T.J. Huffman[a], N.C. Branagan[a], M.M. Qazilbash[a]*, P. Srivastava[b], T. Goehringer[b], G. Yong[b], V. Smolyaninova[b] and R. Kolagani[b]

[a]*Department of Physics, College of William and Mary, Williamsburg, VA 23187-8795, USA;* [b]*Department of Physics, Astronomy and Geosciences, Towson University, Towson, MD 21252, USA*

(*Received 22 July 2014; accepted 1 May 2015*)

Previous infrared studies on the hole-doped manganite $La_{0.67}Sr_{0.33}MnO_3$ (LSMO) have analysed its charge dynamics in terms of one type of charge carrier despite evidence of both electron and hole Fermi surfaces. Here, we investigate the charge dynamics of an LSMO film with infrared and optical spectroscopy in order to provide a complete picture of metallic conduction. In the ferromagnetic metallic phase, the low-frequency optical conductivity is best explained by a two-carrier model comprising electrons and holes. The number densities, effective masses and relaxation response of the delocalized electrons and holes are quantified. We discover that only one-third of the doped charges are coherent and contribute to the dc transport. Metallic LSMO cannot be classified as a bad metal at low temperatures because the mean free path of the coherent, mobile charge carriers exceeds the Ioffe–Regel–Mott limit. The incoherent spectral response of the doped charges manifests itself as a broad mid-infrared feature. We also report the first observation of splitting of an infrared-active phonon due to local Jahn–Teller distortion in the vicinity of the thermally driven transition to the nonmetallic, paramagnetic phase in LSMO. This demonstrates that infrared spectroscopy is capable of detecting the presence of local lattice distortions in correlated electron systems.

**Keywords:** manganite; metal–insulator transition; infrared; optical spectroscopy



## 1. Introduction

The alkaline earth-doped manganites have received considerable attention since the discovery of colossal magnetoresistance in these materials [1]. The class of materials $(Ln)_{1-x}(A)_xMnO_3$ has a pseudocubic perovskite structure (Ln stands for rare earth and A for alkaline earth metals). The phase diagram of the Sr-doped manganite $La_{1-x}Sr_xMnO_3$ is quite complex and diverse exhibiting a variety of structural, electronic and magnetic phases. The parent compound $LaMnO_3$ is a highly correlated insulator that exhibits antiferromagnetic and orbital ordering. Both the on-site Coulomb repulsion and cooperative Jahn–Teller distortion are thought to contribute to the insulating behaviour [2–4]. The Sr doping introduces charge carriers and suppresses the

*Corresponding author. Email: mumtaz@wm.edu

long-range Jahn–Teller effect. Pulsed neutron diffraction provides evidence for local Jahn–Teller distortion for doping levels between 0.16 and 0.4, even though crystallographic analysis does not reveal macroscopic, long-range Jahn–Teller effect [5]. Higher hole carrier number, and loss of both long-range cooperative Jahn–Teller distortion and orbital ordering lead to the emergence of double-exchange driven ferromagnetic metallic phase as the low-temperature ground state for Sr doping levels between 0.17 and 0.5 [6,7].

In this work, we report infrared properties of $La_{1-x}Sr_xMnO_3$ films with doping level $x = 0.33$. This compound has a rhombohedral crystal structure and a ferromagnetic to paramagnetic phase transition near the critical temperature $T_c = 350$ K [7]. Magnetization experiments verify this phase transition is second order [8]. Below $T_c$, the ferromagnetic phase is metallic, while above $T_c$ the paramagnetic phase is nonmetallic and exhibits characteristics of an insulator. The Mn 3*d* orbitals make the most significant impact on the conductive properties of hole-doped manganite with positive Hall coefficient [9]. They are split into $e_g$ and $t_{2g}$ orbitals by the crystal field. The three electrons localized on the $t_{2g}$ orbitals of Mn atom form a core spin of $S_c = 3/2$. The transfer probability of the $e_g$ electrons on the Mn sites depend on their spin states. According to the double-exchange model proposed by Zener [10], in the low-temperature metallic phase, the core spins of Mn sites align with each other. When the $e_g$ electrons transfer between different Mn sites, the scattering probability is minimized because the $e_g$ electrons retain their spin state that is aligned to the Mn core spins. Thus, metallic bonds are formed. Upon raising the temperature, the core spins of Mn sites become randomly oriented, and the mobility of $e_g$ electrons is hampered. The double-exchange model provides one possible explanation for the phase transition between the ferromagnetic metallic state and paramagnetic insulating state with increasing temperature [11].

As pointed out by Millis et al. [12], hopping conductance and Hund's coupling together give an unreasonable value of $T_c$, which is about an order of magnitude higher than the measured values. The magnitude and temperature dependence of the resistivity near $T_c$ estimated with this approach is not consistent with the experimental data either. Thus, the formation of polarons due to the Jahn–Teller effect should be included to explain the insulating phase of $La_{1-x}Sr_xMnO_3$ compounds for $0.16 < x < 0.5$. Indeed the energy gap in the insulating phase of the hole-doped manganites LSMO and $La_{0.67}Ca_{0.33}MnO_3$ has been attributed to the presence of local Jahn–Teller distortion [13,14]. The interaction between the lattice, spin and charge degree of freedoms makes this material a prototype of a complex, correlated system.

The nature of metallic conduction in correlated systems such as $La_{0.67}Sr_{0.33}MnO_3$ (LSMO) is of considerable interest and an outstanding unresolved problem. Certain ferromagnetic manganites are reported as bad metals because they appear to violate the Ioffe–Regel–Mott criterion [15]. Moreover, the optical conductivity in the metallic phase cannot be explained by a simple Drude model alone [15–17]. Based on low-temperature reflection data, we use a Drude mode and two Tauc–Lorentz oscillators to analyse the low-frequency infrared behaviour of an annealed $La_{0.67}Sr_{0.33}MnO_3$ film. Our model considers both electron and hole free carriers as well as localized carriers and differs from previous approaches [15–17] in that it provides a view that is consistent with other reported experimental results [18–24]. Unlike previous infrared studies, our analysis allows us to quantify the dynamical parameters (carrier densities, scattering rates, effective masses and mean free paths) of both electrons and holes. We discover

that LSMO is not a bad metal at low temperatures because the mean free path of the charge carriers exceeds the Ioffe–Regel–Mott limit. We also report the first observation of splitting of an infrared phonon in the LSMO film, which we attribute to local Jahn–Teller distortion. It provides evidence that local lattice distortions in correlated electron systems can be detected with infrared spectroscopy.

## 2. Experimental method

$La_{0.67}Sr_{0.33}MnO_3$ (LSMO) films of thickness ~85 nm were grown on (1 0 0) oriented $LaAlO_3$ (LAO) substrates, employing pulsed laser deposition method using a KrF excimer laser. Films were grown at 800 °C in an oxygen pressure of 400 mTorr and laser fluence ~1.5 J/cm$^2$, and subsequently post-annealed at 800 °C for ~8 h in flowing oxygen to reduce oxygen vacancies and minimize any residual strain due to the compressive mismatch (~1.8 %) between the in-plane lattice constants of LSMO and (1 0 0) $LaAlO_3$. The as-grown and post-annealed films were analysed at room temperature using a four-circle X-ray diffractometer. Films are single phase and (0 0 1) oriented (in cubic index) as indicated by $2\theta$-$\omega$ scans (Figure 1(a)). Rocking angle FWHM's are ~0.2° indicating good crystallinity, and Φ-scans indicate in-plane cube-on-cube in alignment with the substrate. Post-annealing causes a decrease in out-of-plane lattice constant and a concomitant decrease in dc resistivity, consistent both with strain relaxation and

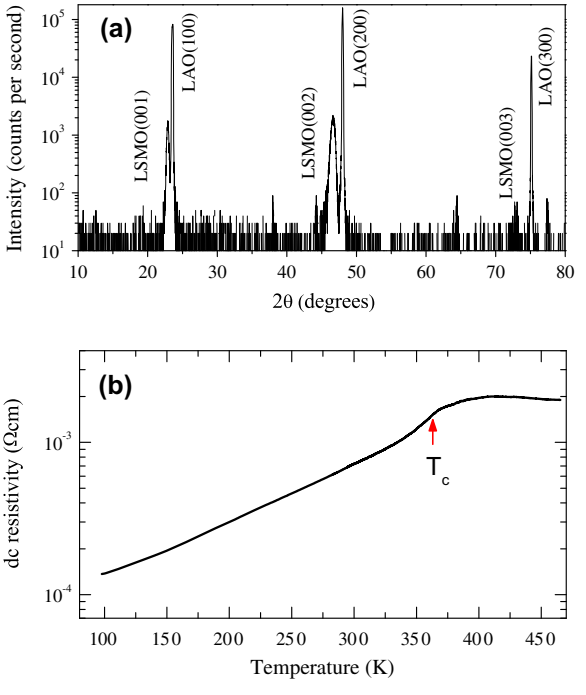


Figure 1. (colour online) (a) X-ray diffraction measurement for annealed $La_{0.67}Sr_{0.33}MnO_3$ film on $LaAlO_3$ substrate. (b) Temperature dependence of dc resistivity of annealed $La_{0.67}Sr_{0.33}MnO_3$ film.

oxygenation. DC resistivity at room temperature in post-annealed films is comparable to the best quality single crystals of LSMO with the same composition [16]. The temperature dependence of the resistivity shows metallic behaviour below room temperature (see Figure 1(b)).

Near normal incidence reflectance measurements were performed on the film-substrate system to obtain the complex dielectric function of the LSMO film. Absolute reflectance data with unpolarized light was acquired in a vacuum Fourier transform infrared (FTIR) spectrometer (VERTEX 80v, Bruker Optics Inc.). A reflectance unit, mechanical translation system and high vacuum equipment have been added to the FTIR spectrometer in order to obtain the reflectance spectra at elevated and cryogenic temperatures. The sample was mounted on a sample holder attached to the end of the cold finger of a variable temperature cryostat. The infrared reflectance data on the oxygen-annealed LSMO film on LAO substrate is obtained from 30 to 400 K with respect to a thick gold film in the spectral range from 60 to 6000 $cm^{-1}$. In addition, room-temperature spectroscopic ellipsometry data from 0.6 eV (~4800 $cm^{-1}$) to 6 eV (~48,000 $cm^{-1}$) was obtained with V-VASE ellipsometer (J. A. Woollam Co. Inc.). The higher frequency ellipsometry data enables a more accurate determination of the complex dielectric function in the infrared spectral range. The infrared and optical properties of the bare LAO substrate were also obtained via the spectroscopic methods described above. The infrared and optical spectroscopy data on the substrate and the LSMO film-substrate system were analysed using WVASE32 software (J. A. Woollam Co. Inc.). Optical conductivity of the LSMO film was obtained by modelling the data with Kramers-Kronig consistent Drude, Lorentz and Tauc–Lorentz oscillators.

The surface morphology of the $La_{0.67}Sr_{0.33}MnO_3$ film has been measured with tapping mode AFM. The analysis of the surface morphology provides important information about surface roughness that is utilized when modelling the optical data. An effective medium layer is used to include the surface roughness in the optical data analysis. The RMS value 1.48 nm of surface roughness for the LSMO film has negligible effect at infrared and visible wavelengths. However, if not taken into account, surface roughness can lead to systematic uncertainty (at 10% level) in the optical constants in the ultraviolet spectral range.

We estimate that the $T_c$ of the insulator to metal transition is about 360 K from the sharp drop in the temperature-dependent dc resistivity data shown in Figure 1(b). The temperature dependence of the dc resistivity of the film is similar to that of a single crystal of comparable doping [16].

## 3. Metallic conductivity

The temperature-dependent reflectance of the annealed $La_{0.67}Sr_{0.33}MnO_3$ film is plotted in Figure 2. The data shows the increase in the reflectance in the far- and mid-infrared with decreasing temperature. The optical conductivity of the LSMO film is shown from 60 to 6000 $cm^{-1}$ for representative temperatures in Figure 3. The low-frequency conductivity at 400 K is consistent with an energy gap in the insulating phase. The increase of the low-frequency conductivity with decreasing temperature reveals the phase transition to a metallic phase. The growth of a narrow Drude-like feature below 200 K is observed. Moreover, as previous researchers have pointed out [15–17], a broad absorption feature

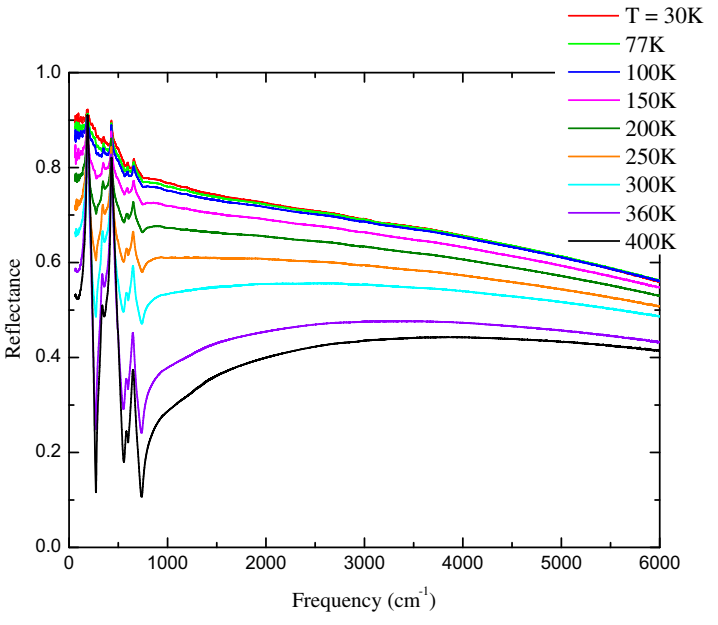


Figure 2. (colour online) Frequency dependence of reflectance of annealed $La_{0.67}Sr_{0.33}MnO_3$ film on $LaAlO_3$ substrate from $T = 30$ to 400 K.

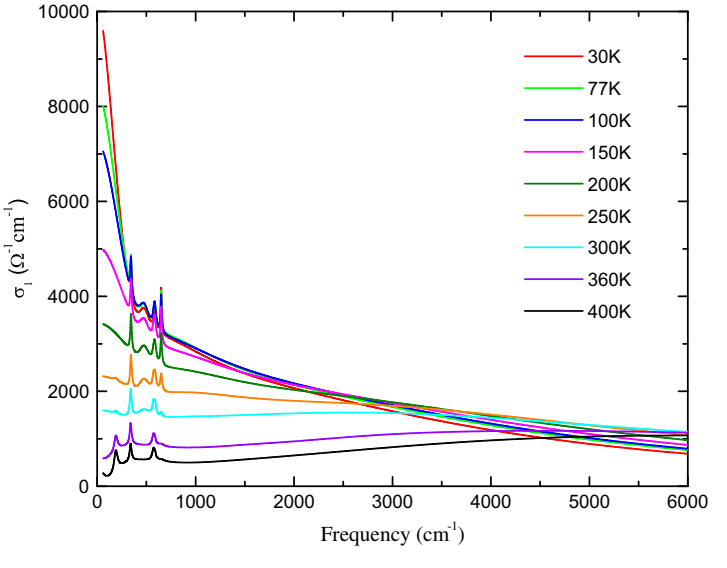


Figure 3. (colour online) Frequency dependence of optical conductivity of annealed $La_{0.67}Sr_{0.33}MnO_3$ film between $T = 30$ and 400 K.

centred about 2500 $cm^{-1}$ in the mid-infrared persists to the lowest measured temperature, and must be considered in a definitive explanation of $La_{0.67}Sr_{0.33}MnO_3$ film's metallic nature.

Previous infrared data in the literature on LSMO were explained with a combination of a simple Drude oscillator and a Lorentz oscillator [16]. However, only one type of carrier is considered contributing to the Drude feature in Ref. [16]. More recently, the extended Drude analysis has been applied by a few researchers instead of the conventional Drude–Lorentz model [15,17]. However, no more than one type of carrier is considered with the extended Drude approach. Existing experimental evidence clearly shows the necessity of considering two types of free carriers. The angle-resolved photoemission spectroscopy (ARPES) data show solid evidence of a nearly spherical electron pocket [18–21]. An electron–positron annihilation experiment measured the nearly cubic structure of the hole pocket in $La_{0.7}Sr_{0.3}MnO_3$ [22]. The sizes and shapes of both the electron and hole Fermi surfaces are consistent with electronic structure calculations [25]. Furthermore, a two-carrier model including both electron and hole carriers can explain the Hall effect data of $La_{0.7}Sr_{0.3}MnO_3$ [23], while an exclusive hole-carrier model will lead to much higher hole density compared with the Sr doping level [9]. Here, we show that two types of free carriers including electrons and holes with nearly equal mobilities need to be taken into consideration to explain the infrared data of metallic LSMO at lower temperatures.

The Hall coefficient [9,23] is positive and nearly temperature independent below 200 K for unstrained LSMO samples with similar doping level to that studied in this work. The simplest explanation for these results is that the hole and electron mobilities are nearly equal and their ratio is independent of temperature. This follows from considering the analytic form for the Hall coefficient:

$$R_{\mathrm{H}} = \frac{r_{\mathrm{h}} n_{\mathrm{h}} \mu_{\mathrm{h}}^2 - r_{\mathrm{e}} n_{\mathrm{e}} \mu_{\mathrm{e}}^2}{e(n_{\mathrm{h}} \mu_{\mathrm{h}} + n_{\mathrm{e}} \mu_{\mathrm{e}})^2} \tag{1}$$

where $r_{\mathrm{h}}$ and $r_{\mathrm{e}}$ are fixed Fermi surface shape factors for holes and electrons, $n_{\mathrm{h}}$, $\mu_{\mathrm{h}}$, $n_{\mathrm{e}}$ and $\mu_{\mathrm{e}}$ are the number density and the mobility of holes and electrons, respectively, and $e$ is the magnitude of the electron charge [23].

If the mobilities of the hole and electron carriers are the same, then the expression for the Hall coefficient is independent of the mobilities:

$$R_{\mathrm{H}} = \frac{r_{\mathrm{h}} n_{\mathrm{h}} - r_{\mathrm{e}} n_{\mathrm{e}}}{e(n_{\mathrm{h}} + n_{\mathrm{e}})^2} \tag{2}$$

$R_{\mathrm{H}}$ now depends only on the carrier densities and the shapes of the Fermi surfaces. This sets the stage for analysis of our infrared reflectance data. We are able to fit the infrared reflectance at and below 200 K to one Drude [26] and two Tauc–Lorentz oscillators [27]. We choose to employ for the fits a minimum number of Kramers–Kronig consistent oscillators and a minimum total number of free parameters. The fits to the reflectance data can also be achieved with a Drude mode and three or more Lorentz oscillators without changing the results of this work. The delocalized carriers contribute to the narrow Drude feature. The quasi-localized charges lead to the broader mid-infrared mode in the optical conductivity which is described by the two Tauc–Lorentz oscillators as shown in Figure 4. The Tauc–Lorentz oscillator is similar to a Lorentz oscillator, but has

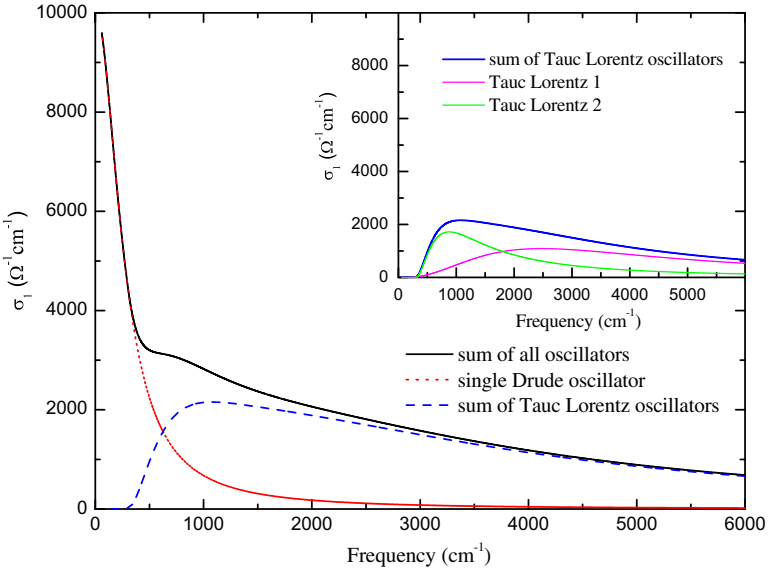


Figure 4. (colour online) The electronic part of the optical conductivity at $T = 30$ K. The optical conductivity consists of the sum of a single Drude oscillator and broad mid-infrared mode. The broad mid-infrared mode is a sum of two Tauc–Lorentz oscillators as shown in the inset.

an additional energy gap parameter. The physical meaning of the small energy gaps of the Tauc–Lorentz oscillators is that the incoherent excitations in metallic LSMO are gapped. This is similar to the broad, gapped mid-infrared mode in the optical conductivity of other correlated electron systems in which there is an energy gap for optical transitions between the localized bands and the conducting band [28].

Only one Drude mode is required to model the free-carrier infrared response. This suggests that the scattering rate (or inverse carrier lifetime) is the same for both electrons and holes at a particular temperature. Moreover, the carrier lifetimes for both electrons and holes have the same temperature dependence because one Drude mode is required to model the free carrier part of the infrared spectra for all temperatures ≤200 K. This fact taken together with the observation of the same mobilities of electrons and holes, tells us that both types of carriers have the same effective masses. From fits to the infrared reflectance data, we obtain the temperature dependence of the plasma frequency and the scattering rate of the free carriers and these quantities are shown in Figure 5.

The plasma frequency has the form $\omega_p = (\frac{4\pi ne^2}{m^*})^{\frac{1}{2}}$ and depends upon the ratio of the free carrier density ($n$) and effective mass ($m^*$). If we take the mass of the carriers to be nearly equal to the free electron mass in accord with the ARPES dispersion near the Fermi energy [18], we find the total free carrier density from our infrared data to be approximately $1.8 \times 10^{21}$ cm$^{-3}$ (0.1 free carriers per Mn site). From the Hall effect data [23], one obtains the ratio of 7:3 for the holes and electron carrier densities assuming identical mobilities. The model of two carriers with nearly equal mobilities and with the holes as majority carriers is qualitatively consistent with a positive and temperature-independent Seebeck coefficient at low temperatures [24,29].

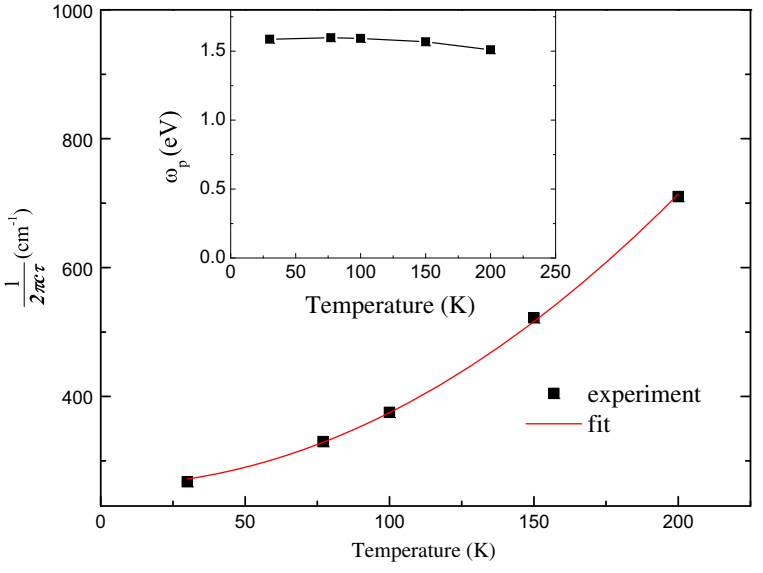


Figure 5. (colour online) The temperature dependence of the scattering rate. Note that the scale of the vertical axis begins at 230 cm$^{-1}$. The inset shows the temperature dependence of the plasma frequency of the Drude mode.

We also attempted to calculate the density of electron and hole carriers from the size of Fermi surfaces measured by ARPES and electron–positron annihilation. The (pseudo-cubic) lattice constant $a$ of LSMO is about 3.9 Å [21]. According to Ref. [19], and references therein, a sphere with radius between $0.43\frac{\pi}{a}$ and $0.48\frac{\pi}{a}$ can be used to estimate the size of the electron pocket. A spin polarization of 50% for the electrons is assumed which is consistent with spin resolved photoemission data [19]. A Fermi surface radius of $0.45\frac{\pi}{a}$ is adopted for calculating the electron carrier density. The hole pocket is approximated by a cube with side length of $0.65\frac{2\pi}{a}$ [22]. Holes, which are the dominant carriers, are treated as completely spin-polarized. This is consistent with the existence of a nearly half-metallic ferromagnetic ground state [30]. Carrier densities of $1.1 \times 10^{21}$ cm$^{-3}$ (0.07 carriers per Mn site) for the electrons and $4.6 \times 10^{21}$ cm$^{-3}$ (0.27 carriers per Mn site) for the holes are obtained from the volume enclosed by the electron and hole Fermi surfaces according to the band structure picture.

However, the free carrier density from infrared data ($1.8 \times 10^{21}$ cm$^{-3}$) is significantly smaller than that obtained from the simple free carrier interpretation of the ARPES and electron–positron annihilation data (approximately $5.7 \times 10^{21}$ cm$^{-3}$, which is approximately 0.34 carriers per Mn site). We explain this difference by postulating that about one-third of carriers in the electron and hole pockets are actually mobile, while the remaining majority are localized due to charge and magnetic correlation effects. Averaged to every Mn site, approximately 0.1 free carriers are obtained compared to 0.33 expected based on the Sr concentration. This again justifies our assertion that the mid- infrared absorption comes from localization induced by correlation effects. If we assume that both free and localized charge carriers have effective masses almost equal to the bare electron mass, the number density of charge carriers obtained by integrating the optical

conductivity below 6000 $cm^{-1}$ at low temperatures is approximately $5 \times 10^{21}$ $cm^{-3}$, which accounts for nearly all the carriers obtained from the size of the electron and hole pockets within the single particle picture.

The temperature dependence of the relaxation rate of the free carriers is shown in Figure 5. They can be fit by a quadratic curve of the form $A + BT^2$, where $A$ is the residual scattering rate and $B$ is the coefficient of the quadratic term. However, the coefficient of the quadratic temperature-dependent term obtained from the fit is $1.88 \times 10^9$ $K^{-2}s^{-1}$, which is about 270 times larger than the value of $6.95 \times 10^6$ $K^{-2}s^{-1}$ in Au which is a good metal. We also note the large residue scattering in the limit of low temperatures in LSMO [31]. To estimate the mean free path of the free carriers, we assume both electron and holes have approximately equal Fermi velocity $5 \times 10^5$ m $s^{-1}$obtained from the measured dispersion in the ARPES data. Then the mean free path is approximately 10 nm at 30 K and 3.5 nm at 200 K compared with the Fermi wavelength of 1.4 nm and lattice constant about 3.9 Å. At 200 K and lower temperatures, the mean free path of the coherent carriers exceeds the Ioffe–Regel–Mott limit, and this implies that metallic LSMO is not a bad metal. Our model cannot be applied to the conductivity above 200 K because of the expected instability towards insulating behaviour and possible phase separation. We note that the quadratic temperature dependence of the scattering rate with an anomalously large coefficient ($B$), may be qualitatively explained within the framework of the hidden Fermi liquid picture [32]. At the same time, the large residual scattering at very low temperatures would also need to be accounted for in a realistic theoretical model. Besides scattering due to impurities, the many body effects involving dynamical electron–electron interactions may make significant contribution to the low-temperature residual scattering rate observed in our experiments [33]. We also note that the spectral weight of the Drude mode has a weak temperature dependence below 200 K (see inset of Figure 5), which is consistent with the nearly temperature-independent Hall and Seebeck coefficients. There is also a mild increase (less than 10%) in the spectral weight of the mid-infrared feature with decreasing temperature and this can be explained by spectral weight transfer from higher frequencies.

We also attempted to fit the infrared reflectance data with two Drude oscillators, one narrow and the other quite broad. A reasonable fit was obtained and two possible scenarios were explored. First, the narrow Drude was assumed to arise from hole carriers and the broad Drude from the electron carriers. The second scenario was to reverse the assignment of the two Drude oscillators. However, neither scenario gave results that were consistent with the Hall effect measurements of Ref. [23] indicating that these alternative models are not realistic.

## 4. Infrared-active phonons

The rhombohedral primitive cell of $La_{0.67}Sr_{0.33}MnO_3$ contains 10 atoms and corresponds to 30 phonon modes. Group theory predicts that the rhombohedral crystal exhibits eight infrared-active phonon modes $3A_{2u} + 5E_u$ and five Raman-active phonon modes $A_{1g} + 4E_g$. Including five silent modes $2A_{1u} + 3A_{2g}$ and three acoustic modes, there are a total of 30 modes including doubly degeneracy of $E_u$ and $E_g$ modes [34]. Our thin film has the orientation of (0 0 1) in cubic notation. The [1 1 1] axis of the rhombohedral unit cell coincident with the [1 1 1] axis of the cubic cell aligns with an

angle about 35° relative to the sample surface. However, the optical anisotropy of LSMO can be better described with a hexagonal unit cell instead of the rhombohedral primitive cell. The $c_h$ axis of the larger hexagonal cell is in the same direction as the [1 1 1] axis of the rhombohedral cell [35]. Four possible rhombohedral domains induced by twinning exist in the film [35]. As a result, all eight infrared-active phonon modes could be observed in principle.

The infrared-active phonon modes of annealed $La_{0.67}Sr_{0.33}MnO_3$ film are shown in Figure 6. The phonon features were modelled with Lorentz oscillators. We can clearly resolve only the most prominent phonons around 340 and 580 $cm^{-1}$ in the reflectance spectra. Both of them are $A_{2u}$ modes. The 340 $cm^{-1}$ is the bending mode and the 580 $cm^{-1}$ is the stretching mode [36]. The polarization of the $A_{2u}$ mode phonons is along the [1 1 1] direction of the cubic cell and thus the $c_h$ direction of the hexagonal unit cell [37]. As a result, they can be clearly resolved by our near normal reflectance measurement with unpolarized light. The reasons that other phonons cannot be clearly resolved are following: lower signal from the film whose thickness is much less than infrared wavelengths, the presence of strong phonon features of LAO substrate and the screening effect of mobile charges in the metallic phase. The oscillator parameters of the 340 $cm^{-1}$ infrared phonon mentioned above agrees with previous reported results [36,38,39]. The inclusion of two additional Lorentzian oscillators was required in order to improve the fits to the data and these oscillators likely correspond to infrared-active phonons. The infrared phonon around 200 $cm^{-1}$ is present in the insulating phase, but it is heavily screened by the high reflectivity of metallic electrons and cannot be resolved at lower temperatures. The oscillator parameters for the phonon at 650 $cm^{-1}$

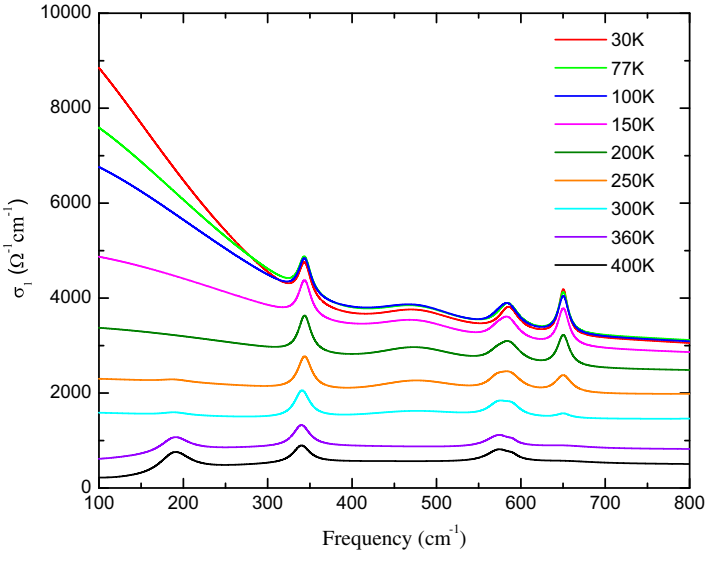


Figure 6. (colour online) Frequency dependence of the optical conductivity of $La_{0.67}Sr_{0.33}MnO_3$ film measured at different temperatures from $T = 30$ to 400 K. The phonon features between 100 and 800 $cm^{-1}$ are shown.

have some uncertainty because the oscillator frequency coincides with that of the strong phonon feature from LAO substrate.

We emphasize the observation of the splitting of infrared phonon around 580 $cm^{-1}$ in $La_{0.67}Sr_{0.33}MnO_3$ film that has not been reported in earlier works to the best of our knowledge. We are able to resolve this splitting due to the high spectral resolution of 2 $cm^{-1}$ used to obtain the data. We zoom in on the 580 $cm^{-1}$ infrared phonon shown in Figure 7(a), and we see that the phonon peaks are separated by 17 $cm^{-1}$. This phonon is a stretching mode which is more easily visualized and discussed in a pseudo-cubic unit cell [38,40]. The main characteristic feature of the stretching mode is that the manganese atom within the oxygen octahedra moves against the oxygen atoms in the axial direction. This phonon mode usually corresponds to higher frequency than the bending mode which has the manganese atom and the axial oxygen atoms moving along the same direction, but against the four oxygen atoms within the horizontal plane. These two modes are sensitive to the bond length and strength along the axial direction connecting the oxygen atoms and manganese atom. The infrared phonon splitting observed in our experiment can be explained by local Jahn–Teller distortion, which modifies the bond length and strength along the axial direction of the oxygen octahedra. The Jahn–Teller effect in the paramagnetic insulating phase distorts the oxygen octahedra making the Mn–O bond length larger along the axial direction. Since hole doping by Sr leads to empty $e_g$ orbitals on the $Mn^{4+}$ sites, the oxygen octahedra surrounding these sites are not expected to show Jahn-Teller distortion. This distortion is reduced as the film becomes



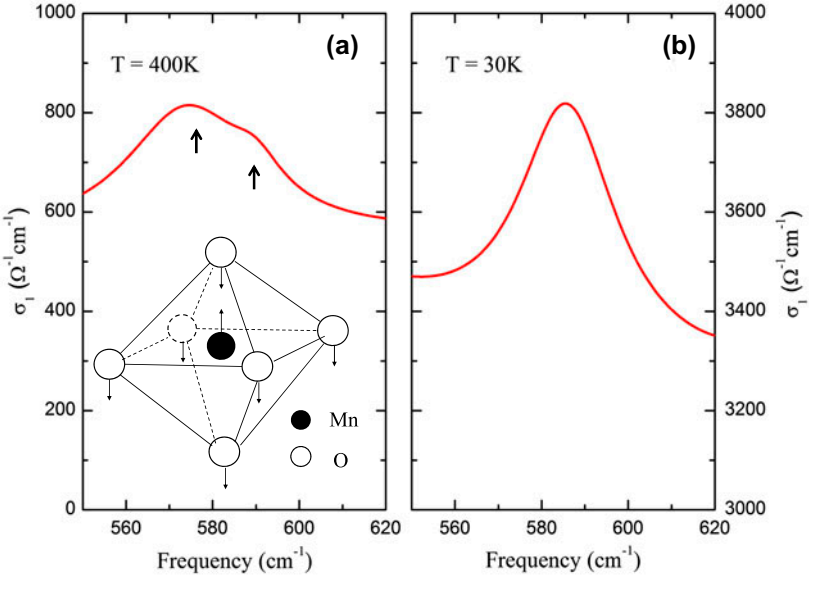


Figure 7. (colour online) (a) Optical conductivity at $T = 400$ K shows splitting of the stretching mode phonon due to Jahn–Teller distortion. The two arrows are displayed at the centre frequencies of 573 and 590 $cm^{-1}$ of two Lorentz oscillators that were used to model the phonon doublet. A schematic figure of the stretching mode vibration is shown in the inset. (b) Optical conductivity at $T = 30$ K shows a single phonon mode.

ferromagnetic metallic and subsequently vanishes at the lowest temperatures. Our observations thus confirm previous reports of these phenomena including both PDF analysis and XAFS experiments [41–43]. The local Jahn–Teller distortion is randomly oriented [42]. Thus, the Sr doping introduces random distribution of undistorted oxygen octahedra and different bond length and strength along the axial direction within the oxygen octahedra in the insulating regions. The mixed distribution of the different kinds of Mn–O bonds along the axial direction splits the stretching phonon near 580 $cm^{-1}$.

The phonon splitting that we observe is quite similar to that observed by Barker *et al*. in mixed $KMgF_3$–$KNiF_3$ crystal [44]. The random distribution of different bonds caused by the random distribution of Mg and Ni is not simply described as a macroscopic combination of the dielectric function of two different materials. The mixed $KMgF_3$–$KNiF_3$ crystal also has perovskite structure with Mg and Ni atoms at the same locations as Mn in our LSMO system. The phonon splitting observed in the reststrahlen band within the 200 and 300 $cm^{-1}$ region in the mixed $KMgF_3$–$KNiF_3$ crystal corresponds to the stretching mode, a counterpart of the situation in LSMO. The main difference is that the phonon splitting of the mixed $KMgF_3$–$KNiF_3$ crystal involves mass difference of Mg and Ni atoms and variation of the bond strength, while in LSMO only the variation of bond strength is involved. The phonon splitting will remain in the hypothetical situation in which the Ni atom is replaced by a much lighter atom with similar mass to Mg atom, but with the bond strengths unchanged and Grüneisen constant non zero [44]. This hypothetical situation is exactly the analogy to what we meet in our LSMO system. Thus, the phonon splitting observed in LSMO can be qualitatively explained within the framework of the mixed crystal theory once changes in bonding caused by local Jahn–Teller distortion are taken into consideration. The disappearance of the phonon splitting at low temperatures as see in Figure 7(b) is consistent with the vanishing of Jahn–Teller distortion deep into the metallic phase.

## 5. Conclusions

We performed temperature-dependent infrared spectroscopy on an annealed $La_{0.67}Sr_{0.33}MnO_3$ film grown on (1 0 0) $LaAlO_3$ substrate. The electronic part of the optical conductivity is modelled with one Drude and two Tauc–Lorentz oscillators. Our analysis is consistent with the presence of hole and electron carriers in metallic LSMO, and by reconciling our infrared data with Hall effect, ARPES and electron–positron annihilation experiments, we find that these two types of carriers have essentially similar dynamical properties. Thus, we provide a complete picture of metallic conduction in LSMO including quantitative values of the dynamical parameters and number densities of both electron and hole charge carriers. Our results indicate that only one-third of the doped charges in LSMO are mobile. The mean free path of the mobile carriers exceeds the Ioffe–Regel–Mott limit of metallic transport and therefore metallic LSMO cannot be regarded as a bad metal. The majority of the doped charges are localized due to many-body correlation effects and appear as a broad mid-infrared feature in the optical conductivity. Our analysis reveals a quadratic temperature dependence of the scattering rates of both electrons and holes, consistent with the recently proposed "hidden Fermi liquid" model [32]. We report the first observation of splitting of the stretching phonon mode induced by local Jahn–Teller distortion in this material. We provide an explanation of this phenomenon based on the mixed crystal theory [44]. Our

work provides evidence that infrared spectroscopy can be utilized to detect local lattice distortions in correlated electron systems.

## Acknowledgement

The authors acknowledge experimental assistance by Chris Jensen in the measurement of the dc resistivity of $La_{0.67}Sr_{0.33}MnO_3$.

## Disclosure statement

No potential conflict of interest was reported by the authors.

## Funding

This work was supported by the NSF DMR [grant number 1255156]; the Jeffress Memorial Trust; the NSF ECCS [grant number 1128586].



## References

[1] E. Dagotto, *Nanoscale Phase Separation and Colossal Magnetoresistence*, Springer, Berlin, 2002.
[2] N. Kovaleva, A. Boris, C. Bernhard, A. Kulakov, A. Pimenov, A. Balbashov, G. Khaliullin and B. Keimer, Phys. Rev. Lett. 93 (2004) p.147204.
[3] J. Kanamori, J. Appl. Phys. 31 (1960) p.S14.
[4] T. Hotta, S. Yunoki, M. Mayr and E. Dagotto, Phys. Rev. B 60 (1999) p.R15009.
[5] D. Louca and T. Egami, J. Appl. Phys. 81 (1997) p.5484.
[6] M. Paraskevopoulos, F. Mayr, J. Hemberger, A. Loidl, R. Heichele, D. Maurer, V. Müller, A.A. Mukhin and A.M. Balbashov, J. Phys.: Condens. Matter 12 (2000) p.3993.
[7] J. Hemberger, A. Krimmel, T. Kurz, H.-A. Krug von Nidda, V. Ivanov, A. Mukhin, A.M. Balbashov and A. Loidl, Phys. Rev. B 66 (2002) p.094410.
[8] J. Mira and J. Rivas, Phys. Rev. B. 60 (1999) p.2998.
[9] A. Asamitsu and Y. Tokura, Phys. Rev. B. 58 (1998) p.47.
[10] C. Zener, Phys. Rev. 82 (1951) p.403.
[11] H. Yi and J. Yu, Phys. Rev. B 58 (1998) p.11123.
[12] A.J. Millis, P.B. Littlewood and B.I. Shraiman, Phys. Rev. Lett. 74 (1995) p.5144.
[13] M. Quijada, J. Černe, J.R. Simpson, H.D. Drew, K.H. Ahn, A.J. Millis, R. Shreekala, R. Ramesh, M. Rajeswari and T. Venkatesan, Phys. Rev. B 58 (1998) p.16093.
[14] J.H. Jung, K.H. Kim, T.W. Noh, E.J. Choi and J. Yu, Phys. Rev. B 57 (1998) p.11043.
[15] A. Haghiri-Gosnet, M. Koubaa, A. Santander-Syro, R. Lobo, P. Lecoeur and B. Mercey, Phys. Rev. B 78 (2008) p.115118.
[16] Y. Okimoto, T. Katsufuji, T. Ishikawa, T. Arima and Y. Tokura, Phys. Rev. B 55 (1997) p.4206.
[17] K. Takenaka, R. Shiozaki and S. Sugai, Phys. Rev. B 65 (2002) p.184436.
[18] A. Chikamatsu, H. Wadati, H. Kumigashira, M. Oshima, A. Fujimori, M. Lippmaa, K. Ono, M. Kawasaki and H. Koinuma, Phys. Rev. B 76 (2007) p.201103R.
[19] J. Krempaský, V. Strocov, L. Patthey, P. Willmott, R. Herger, M. Falub, P. Blaha, M. Hoesch, V. Petrov, M.C. Richter, O. Heckmann and K. Hricovini, Phys. Rev. B 77 (2008) p.165120.
[20] A. Chikamatsu, H. Wadati, H. Kumigashira, M. Oshima, A. Fujimori, N. Hamada, T. Ohnishi, M. Lippmaa, K. Ono, M. Kawasaki and H. Koinuma, Phys. Rev. B 73 (2006) p.195105.

[21] J. Krempaský, V.N. Strocov, P. Blaha, L. Patthey, M. Radović, M. Falub, M. Shi and K. Hricovini, J. Electron Spectros. Relat. Phenom. 181 (2010) p.63.
[22] E.A. Livesay, R.N. West, S.B. Dugdale, G. Santi and T. Jarlborg, J. Phys.: Condens. Matter 11 (1999) p.L279.
[23] I.M. Dildar, C. Beekman, X. He and J. Aarts, Phys. Rev. B 85 (2012) p.205103.
[24] A. Asamitsu, Y. Moritomo and Y. Tokura, Phys. Rev. B 53 (1996) p.R2952.
[25] W.E. Pickett and D.J. Singh, J. Magn. Magn. Mater. 172 (1997) p.237.
[26] M. Dressel and G. Grüner, *Electrodynamics of Solids*, Cambridge University Press, Cambridge, 2002.
[27] G.E. Jellison and F.A. Modine, Appl. Phys. Lett. 69 (1996) p.371.
[28] M.J. Rozenberg, G. Kotliar, H. Kajueter, G.A. Thomas, D.H. Rapkine, J.M. Honig and P. Metcalf, Phys. Rev. Lett. 75 (1995) p.105.
[29] T. Hashimoto, R. Hirasawa, T. Yoshida, Y. Yonemura, J. Mizusaki and H. Tagawa, Phys. Rev. B 51 (1995) p.576.
[30] M.B. Salamon and M. Jaime, Rev. Mod. Phys. 73 (2001) p.583.
[31] J. Simpson, H. Drew, V. Smolyaninova, R. Greene, M. Robson, A. Biswas and M. Rajeswari, Phys. Rev. B 60 (1999) p.R16263.
[32] W. Xu, K. Haule and G. Kotliar, Phys. Rev. Lett. 111 (2013) p.036401.
[33] V.U. Nazarov, G. Vignale and Y.-C. Chang, Phys. Rev. B 89 (2014) p.241108.
[34] M.V. Abrashev, A.P. Litvinchuk, M.N. Iliev, R.L. Meng, V.N. Popov, V.G. Ivanov, R.A. Chakalov and C. Thomsen, Phys. Rev. B. 59 (1999) p.4146.
[35] M. Zhang, X.L. Ma and D.X. Li, Philos. Mag. 85 (2005) p.1625.
[36] C. Hartinger, F. Mayr, A. Loidl and T. Kopp, Phys. Rev. B 71 (2005) p.184421.
[37] P. Delugas, V. Fiorentini and A. Filippetti, Phys. Rev. B 71 (2005) p.134302.
[38] C. Hartinger, F. Mayr, A. Loidl and T. Kopp, Phys. Rev. B 70 (2004) p.134415.
[39] P. Dore, A. Funaro, A. Sacchetti, M. Angeloni, G. Balestrino, Eur. Phys. J. B 37 (2003) p.339.
[40] J.T. Last, Phys. Rev. 105 (1957) p.1740.
[41] T. Shibata, B. Bunker and J. Mitchell, Phys. Rev. B 68 (2003) p.024103.
[42] D. Louca and T. Egami, Phys. Rev. B 59 (1999) p.6193.
[43] D. Louca, T. Egami, E.L. Brosha, H. Röder and A.R. Bishop, Phys. Rev. B 56 (1997) p.R8475.
[44] A.S. Barker, J. Ditzenberger and H.J. Guggenheim, Phys. Rev. 175 (1968) p.1180.